
# Changes in atmospheric circulation amplify extreme snowfall fueled by Arctic sea ice loss over high-latitude land

Weather and Climate Extremes 50 (2025) 100802

Contents lists available at ScienceDirect

Weather and Climate Extremes

journal homepage: www.elsevier.com/locate/wace

# Changes in atmospheric circulation amplify extreme snowfall fueled by Arctic sea ice loss over high-latitude land

Yubo Liu [a,b,c], Qiuhong Tang [a,b,*], L. Ruby Leung [d], Deliang Chen [e], Jennifer A. Francis [f], Chi Zhang [g], Hans W. Chen [h], Steven C. Sherwood [c,i]

[a] Key Laboratory of Water Cycle and Related Land Surface Processes, Institute of Geographic Sciences and Natural Resources Research, Chinese Academy of Sciences, Beijing, China
[b] University of Chinese Academy of Sciences, Beijing, China
[c] Climate Change Research Centre, University of New South Wales Sydney, Sydney, New South Wales, Australia
[d] Atmospheric, Climate, & Earth Sciences Division, Pacific Northwest National Laboratory, Richland, WA, USA
[e] Department of Earth System Science, Tsinghua University, Beijing, China
[f] Woodwell Climate Research Center, Falmouth, MA, USA
[g] Key Laboratory of Land Surface Pattern and Simulation, Institute of Geographic Sciences and Natural Resources Research, Chinese Academy of Sciences, Beijing, China
[h] Department of Space, Earth and Environment, Chalmers University of Technology, Gothenburg, 41296, Sweden
[i] ARC Centre of Excellence for Climate Extremes, University of New South Wales Sydney, Sydney, New South Wales, Australia

ARTICLE INFO

*Keywords:*
Arctic moisture
Extreme snowfall
Atmospheric circulation
Anthropogenic forcing

ABSTRACT

Arctic sea-ice retreat has been linked to increased winter precipitation and heavy snowfall over land, likely due to a combination of enhanced evaporation from ice-free Arctic marginal seas (AMS) and changes in atmospheric circulation. However, their relative roles and contributions remain uncertain. Here, we show that a greater proportion of AMS evaporative moisture reached high-latitude land during the cold seasons from 1980–1989 to 2012–2021. Atmospheric circulation changes added an additional 13 % increase in the AMS moisture contribution, accounting for 11 % of the total increase in AMS-sourced land precipitation. Notably, 46 % of the increase in AMS-sourced extreme snowfall is attributed to circulation-driven landward moisture transport, representing an 84 % increase beyond the effect of enhanced AMS evaporation alone. Further analysis indicates that both the rise in Arctic moisture and the atmospheric circulation shifts are primarily driven by anthropogenic forcing. These findings highlight how atmospheric circulation changes amplify extreme snowfall fueled by AMS evaporation, underscoring the synergistic effects of Arctic sea ice loss and circulation change on high-latitude winter precipitation.

## 1. Introduction

Arctic sea ice acts as a natural barrier, limiting the exchange of water vapor and energy between the ocean and atmosphere. However, Arctic warming has shortened the time between autumn freeze-up and spring melt (Boisvert and Stroeve, 2015), reducing sea-ice extent to roughly half of its 1980s levels (Liu et al., 2022; Stroeve and Notz, 2018; Stroeve et al., 2012). The increased open water exposure has enhanced atmospheric moisture availability (Ghatak and Miller, 2013; Ridley et al., 2023), contributing to rising precipitation across the Arctic and surrounding regions (McCrystall et al., 2021; Müller et al., 2022; Sato et al., 2022). These shifts can significantly affect high-latitude ecosystems and regional economies (Dial et al., 2024; Luo et al., 2024).

The impact of heightened Arctic evaporation on increased precipitation has garnered considerable attention, with several studies quantifying its effects using water budget approaches (Bailey et al., 2021; Choi et al., 2023; Liu et al., 2024; Müller et al., 2022; Wegmann et al., 2015). Since the early 1990s, more than half of Arctic Ocean precipitation has come from local evaporation (Ford and Frauenfeld, 2022), marking a shift in moisture sources from long-range transport—mainly from the North Atlantic, the subpolar North Pacific, and the Labrador Sea (Dufour et al., 2016; Papritz et al., 2022; Vázquez et al., 2016)—to local recycling. Projections indicate that surface evaporation will continue to drive most of Arctic precipitation increases this century

* Corresponding author. Key Laboratory of Water Cycle and Related Land Surface Processes, Institute of Geographic Sciences and Natural Resources Research, Chinese Academy of Sciences, Beijing, China.
*E-mail address:* tangqh@igsnrr.ac.cn (Q. Tang).

https://doi.org/10.1016/j.wace.2025.100802
Received 28 April 2025; Received in revised form 29 August 2025; Accepted 4 September 2025
Available online 5 September 2025

(Bintanja and Selten, 2014). The effects can extend further southward, influencing precipitation patterns across Northern Hemisphere continents, particularly in Eurasia and North America (Liu et al., 2012; Sato et al., 2022; Wegmann et al., 2015). Since 1980, rising Arctic evaporation has led to about a one-third increase in cold-season Arctic-sourced precipitation over land (Liu et al., 2024), with more intense snowfall over Europe linked to enhanced Barents Sea evaporation (Bailey et al., 2021).

Among extratropical regions, the Arctic shows the most pronounced winter precipitation changes (Pithan and Jung, 2021). While the Arctic Ocean's enhanced evaporation is a major factor, high-latitude precipitation is also shaped by interactions between thermodynamics and atmospheric dynamics. These include direct responses to Arctic sea-ice loss, such as an increased Arctic low cloud cover (Nygård et al., 2019; Ridley et al., 2023), stronger surface winds due to reduced roughness and weaker atmospheric stratification (Zapponini and Goessling, 2024), and more active synoptic-scale cyclone development caused by destabilized atmospheric conditions and latent heating (Crawford et al., 2022). These processes can influence precipitation across the Arctic and nearby regions. For instance, a northwestward shift of southerly flow has intensified extreme precipitation over Svalbard (Müller et al., 2022). Cyclone intensity and frequency changes have increased snowfall over Greenland (Bailey and Hubbard, 2025; Sellevold et al., 2022), while anticyclonic circulation over the Barents–Kara Seas has strengthened northerly winds and driven deeper cold air intrusions into Eurasia (Liu et al., 2025). In addition, changes in Arctic circulation can exert broad and complex influences on weather in lower latitudes. Sea-ice variability influences the position and strength of the stratospheric polar vortex (Kretschmer et al., 2020; Zou and Zhang, 2024), altering the jet stream's waviness (Chripko et al., 2021; Levine et al., 2021; Yu et al., 2024) and modulating mid-latitude westerlies (Screen et al., 2018; Smith et al., 2022), which in turn affect remote precipitation patterns (Liu et al., 2012).

Atmospheric circulation plays a central role in governing the distribution of moisture and shaping regional precipitation patterns. Under the influence of climate changes induced by anthropogenic forcing (Liu et al., 2025) and natural variability (Ding et al., 2019; Topál and Ding, 2023), the patterns of this moisture transport by circulation are not static. In this context, the observed precipitation changes may not correspond proportionately to the increase in Arctic evaporation. The relative contribution of circulation changes is still unclear, raising questions about the mechanisms linking sea-ice retreat and land moistening. Specifically, is the moistening mainly caused by increased evaporation from the ice-diminished Arctic marginal seas, or by favorable atmospheric circulation patterns that enhance moisture transport? If the altered evaporation rate is the dominant factor, land effects would largely depend on the pace of Arctic warming and sea-ice retreat. If circulation changes play a dominant role, enhanced convergence could result in spatially uneven precipitation changes and a greater risk of extreme events, with consequences for water resources, infrastructure, ecosystems, and human health.

In this study, we focus on changes in cold-season precipitation (October–March) over Northern Hemisphere land that originate from Arctic marginal seas (AMS; see Fig. S1a), where sea-ice retreat has significantly increased surface evaporation. To capture long-term changes associated with Arctic warming and sea-ice loss, we compare AMS-sourced land precipitation and extreme snowfall between two key decades: 1980–1989 (the 1980s), the earliest with reliable satellite data, and 2012–2021 (the 2010s), representing recent conditions (Fig. S1b). The respective roles of changes in AMS evaporation and atmospheric circulation are evaluated, and their relative contributions are estimated through a comparative analysis of simulation results under different evaporation and circulation scenarios. Using simulations from the sixth phase of the Coupled Model Intercomparison Project (CMIP6), the underlying mechanisms and anthropogenic impact behind the moistening over land induced by sea-ice retreat are further explored.

## 2. Data and methods

### 2.1. Data

Atmospheric and surface data from European Centre for Medium-Range Weather Forecasts Reanalysis v5 (ERA5; Hersbach et al., 2020) were used as inputs to the moisture-tracing model (described below) and for further comparison and analysis for the cold seasons (October–March) during 1980–2021. The superior performance of ERA5 in the Arctic (Avila-Diaz et al., 2021; Barrett et al., 2020; Cai et al., 2024; Graham et al., 2019), attributed to its high resolution and advanced data assimilation scheme, makes it the preferred choice for investigating Arctic moisture transport and its associated atmospheric dynamics in this study over other global atmospheric reanalysis products. Surface and vertically integrated variables include total column water [kg $m^{-2}$], vertical integral of atmospheric water flux [kg $m^{-1}$ $s^{-1}$], surface pressure [Pa], as well as evaporation [mm of water equivalent], total precipitation [mm], and snowfall [mm of water equivalent] accumulated over the data temporal resolution. Variables on pressure levels include geopotential [$m^2$ $s^{-2}$], specific humidity [kg $kg^{-1}$] and horizontal wind field [m $s^{-1}$] on the lower 23 levels from 1000 to 200 hPa. The data were obtained from the Copernicus Climate Data Store (https://climate.copernicus.eu/climate-data-store) on a $1^\circ \times 1^\circ$ grid, using hourly analysis fields to force the model and monthly atmospheric variables for further analysis and comparison with CMIP6. The change in each variable over time was obtained by multiplying the fitted linear slope and the length of the period.

Monthly CMIP6 data cover the historical period from 1980 to 2014 and extend to 2021 using the SSP2-4.5 shared socioeconomic pathways. The variables include horizontal wind [m $s^{-1}$], specific humidity [kg $kg^{-1}$], and geopotential height [m]. For each available CMIP6 model, one member of the historical and SSP2-4.5 simulations was used for the analysis. Detailed information is provided in Table S1.

### 2.2. Moisture tracing model

The AMS-sourced precipitation over land was calculated and numerically tracked by the Water Accounting Model-2layers (WAM-2layers; van der Ent et al., 2014, 2013) based on the water balance principle. The driving data for WAM-2layers include precipitation, evaporation, atmospheric water flux, specific humidity and wind. Moisture evaporated from a given region ($\boldsymbol{\Omega}$) is tagged in the well-mixed atmospheric precipitable water ($\boldsymbol{W}$) and is continuously updated at each grid point ($\boldsymbol{x, y}$) within a certain time step ($\boldsymbol{t}$), according to the balance between its flow with the horizontal wind ($\boldsymbol{u, v}$), moisture recharge from surface evaporation ($\boldsymbol{E}$), loss as precipitation ($\boldsymbol{P}$), exchange ($\boldsymbol{F_V}$) between atmospheric layers ($\boldsymbol{l}$, the bottom or the top layer), and a residual term ($\boldsymbol{\alpha}$) caused by the interpolation of ERA5 input in each time step to ensure the closure of water balance.

$$\frac{\partial W_{l,\Omega}}{\partial t} + \frac{\partial (W_{l,\Omega} u)}{\partial x} + \frac{\partial (W_{l,\Omega} v)}{\partial y} = E_{l,\Omega} - P_{l,\Omega} \pm F_{V,\Omega} + \alpha_{l,\Omega} \quad (1)$$

Evaporation in each month was tracked to the end of the following month to ensure coverage of the atmospheric water vapor lifetime (Gimeno et al., 2021; Zhang et al., 2017). AMS evaporation was tracked with a time step of 4 min to ensure numerical stability.

### 2.3. WAM-2layers model experiments to disentangle the contribution of changes in AMS evaporation and atmospheric circulation

To quantify the total change in AMS-sourced precipitation and to decompose the contribution of changes in AMS evaporation and atmospheric circulation, the atmospheric moisture connections from AMS evaporation to land precipitation were tracked under various scenarios using the WAM-2layers model. An overview of the four experiments is

provided in Table 1. The input variables for the WAM-2layers model include evaporation data, denoted as **E**, and other data such as precipitation, atmospheric water and wind, which are collectively classified as atmospheric circulation data and denoted as **C**. To simplify notation, the 1980s and 2010s are represented by the subscripts 19 and 20, respectively. The $E_{19}C_{19}$ and $E_{20}C_{20}$ model experiments tracked the moisture connections from AMS evaporation to land precipitation during the cold seasons of the 1980s and 2010s, respectively, using the specific evaporation and meteorological data of the corresponding period. The total change in AMS-sourced precipitation ($\Delta \boldsymbol{Pr}_{\boldsymbol{Total}}$) is quantified as the difference between these two experiments.

$$\Delta Pr_{Total} = Pr_{E_{20}C_{20}} - Pr_{E_{19}C_{19}} \tag{2}$$

Two additional scenario simulation experiments were further conducted for isolating the individual contributions of changes in AMS evaporation and atmospheric circulation to the total change. The $E_{20}C_{19}$ experiment applied AMS evaporation rescaled to match the total 2010s evaporation, while retaining all other meteorological fields from the 1980s. Instead of directly substituting the 2010s evaporation, the rescaled evaporation at each AMS grid point (x, y) was generated by multiplying original 1980s $E_{19}(x,y)$ by a grid-wise scaling factor—defined as the constant ratio of the mean evaporation between the 2010s and 1980s cold seasons: $\frac{\overline{E_{20}(x,y)}}{\overline{E_{19}(x,y)}}$. This approach preserves the temporal variability of the 1980s while maintaining physical consistency between evaporation and circulation fields. The scaling was restricted to the AMS region, based on the assumption that the change in evaporation outside of the AMS is unaffected by changes in the sea ice and open water regions. The difference between $E_{20}C_{19}$ and $E_{19}C_{19}$ estimate the changes in AMS-sourced precipitation attributable to the increased evaporation from the AMS ($\Delta \boldsymbol{Pr}_{\boldsymbol{E,Exp\ 1}}$) under the atmospheric circulation conditions of 1980s. While the difference between $E_{20}C_{20}$ and $E_{20}C_{19}$ reveals the additional changes that cannot be achieved through evaporation changes alone, namely the supplementary alterations resulting from atmospheric circulation changes ($\Delta \boldsymbol{Pr}_{\boldsymbol{C,Exp\ 1}}$).

Similarly, the $E_{19}C_{20}$ experiment represents a scenario in which atmospheric circulation conditions remain fixed at 2010s patterns, while evaporation is adjusted to match 1980s levels (with scaling factor $\frac{\overline{E_{19}(x,y)}}{\overline{E_{20}(x,y)}}$). Based on this simulation, an alternative quantification of evaporation contribution ($\Delta \boldsymbol{Pr}_{\boldsymbol{E,Exp\ 2}}$, defined as the difference between $E_{20}C_{20}$ and $E_{19}C_{20}$) and circulation contribution ($\Delta \boldsymbol{Pr}_{\boldsymbol{C,Exp\ 2}}$, defined as the difference between $E_{19}C_{20}$ and $E_{19}C_{19}$) can be derived.

The total change in AMS-sourced precipitation can be decomposed as the following equation (3). Changes in open water areas and the associated evaporation from the AMS are considered evaporation-driven, although they may be influenced by circulation. Similarly, circulation-induced changes are treated as dynamic, despite potential effects from the evaporation over open water. Owing to inherent nonlinearities in the climate system, $\Delta \boldsymbol{Pr}_{\boldsymbol{E,Exp\ 1}}$ and $\Delta \boldsymbol{Pr}_{\boldsymbol{E,Exp\ 2}}$ (similarly, $\Delta \boldsymbol{Pr}_{\boldsymbol{C,Exp\ 1}}$ and $\Delta \boldsymbol{Pr}_{\boldsymbol{C,Exp\ 2}}$) are not identical, with their discrepancy reflecting the coupled responses between evaporation and circulation changes. These paired estimates can thus be interpreted as providing a plausible range for the contribution of each factor. Consequently, the average of these two estimates is adopted as the optimal representation of the evaporation-induced component ($\overline{\Delta \boldsymbol{Pr}_{\boldsymbol{E}}}$) or the circulation-induced component ($\overline{\Delta \boldsymbol{Pr}_{\boldsymbol{C}}}$).

$$\Delta Pr_{Total} = \Delta Pr_{E,Exp\ 1} + \Delta Pr_{C,Exp\ 1} = \Delta Pr_{E,Exp\ 2} + \Delta Pr_{C,Exp\ 2} = \overline{\Delta Pr_E} + \overline{\Delta Pr_C} \tag{3}$$

The significance of differences between each experiment is assessed using the two-sided Student's t-test.

**Table 1**
Overview of the WAM-2layers model experiments.

| Experiment number | Abbreviation | Evaporation conditions | Circulation conditions |
|---|---|---|---|
| Norm1 | $E_{19}C_{19}$ | Evaporation in the 1980s | Circulation in the 1980s |
| Norm2 | $E_{20}C_{20}$ | Evaporation in the 2010s | Circulation in the 2010s |
| Exp1 | $E_{20}C_{19}$ | Evaporation increased to the amount in the 2010s | Circulation remains the same as in the 1980s |
| Exp2 | $E_{19}C_{20}$ | Evaporation remained the same amount in the 1980s | Circulation changed to that in the 2010s |

## 3. Results

### 3.1. Disentangling the contributions of changes in AMS evaporation and atmospheric circulation to AMS-sourced land precipitation

During the cold seasons, precipitation over mid- to high-latitude land areas exhibited an extensive increase in the 2010s compared with the 1980s (Fig. S1a). Specifically, AMS-sourced precipitation over Northern Hemisphere land areas increased significantly from 82.0 Gt mon$^{-1}$ in the 1980s ($E_{19}C_{19}$) to 104.2 Gt mon$^{-1}$ in the 2010s ($E_{20}C_{20}$), representing a 27 % increase and an absolute gain of 22.2 Gt mon$^{-1}$ (Fig. S2). During the same period, total AMS evaporation increased significantly by 80.2 Gt mon$^{-1}$, despite localized declines in certain regions, such as the Beaufort Sea (Fig. S1a). Assuming fixed atmospheric circulation patterns, the evaporation-induced contribution (Fig. 1a) shows widespread increases across the Northern Hemisphere, with particularly pronounced enhancements over much of high-latitude Eurasia, northeastern Canada, and Greenland. The augmented evaporation from the AMS is estimated to have elevated its moisture contribution to Northern Hemisphere land precipitation by an average of 19.7 Gt mon$^{-1}$ ($\overline{\Delta Pr_E}$; Fig. 1c), with values ranging from 19.3 Gt mon$^{-1}$ ($\Delta Pr_{E,Exp\ 1}$) to 20.1 Gt mon$^{-1}$ ($\Delta Pr_{E,Exp\ 2}$) suggesting potential interaction effects. The increase driven by enhanced evaporation accounted for 89 % of the total AMS-sourced precipitation growth.

Both comparative experiments consistently demonstrate that changes in atmospheric circulation further intensified the contribution of AMS moisture to sustaining land precipitation, 2.5 Gt mon$^{-1}$, averaging from 2.9 Gt mon$^{-1}$ ($\Delta Pr_{C,Exp\ 1}$) and 2.2 Gt mon$^{-1}$ ($\Delta Pr_{C,Exp\ 2}$). This represents an extra 13 % increase in the AMS moisture contribution on top of the enhanced evaporation from the AMS, attributable to atmospheric circulation changes (ranging from 11 % to 15 %). The atmospheric circulation dynamics increased the proportion of AMS-sourced moisture toward land, while the proportion above the ocean decreased accordingly. This circulation-induced increase in AMS-sourced precipitation accounts for 11 % of the total change between the two periods. The spatial pattern shows that, unlike the pervasive positive changes brought about by enhanced evaporation from the source, the influence of atmospheric circulation exhibits marked regional heterogeneity (Fig. 1b). In the Nordic region, eastern Siberia, Alaska, and western Canada, circulation changes provided additional AMS moisture. Regional statistics reveal that across the Eastern Eurasia as well as Alaska and Western Canada within 50–80°N (Fig. S3a), circulation-induced additional AMS moisture supply accounts for approximately half of the evaporation-enhanced moisture contribution (Fig. S3b). Furthermore, at certain grid points over the Russian Far East, Alaska and southwestern Canada and North America, the additional moisture resulting from atmospheric circulation changes even exceeded that from increased evaporation, serving as the dominant factor in the increased AMS-sourced precipitation. Conversely, reductions were observed along the Davis Strait coast, Central Siberia, and most of the mid-latitude Eurasian continent in Fig. 1b. Therefore, the cancelling effects of atmospheric circulation changes are evident over the Central Eurasia between 50 and 80°N (Fig. S3b). In the mid-latitude Eurasia, the circulation-driven suppression of Arctic moisture transport is the

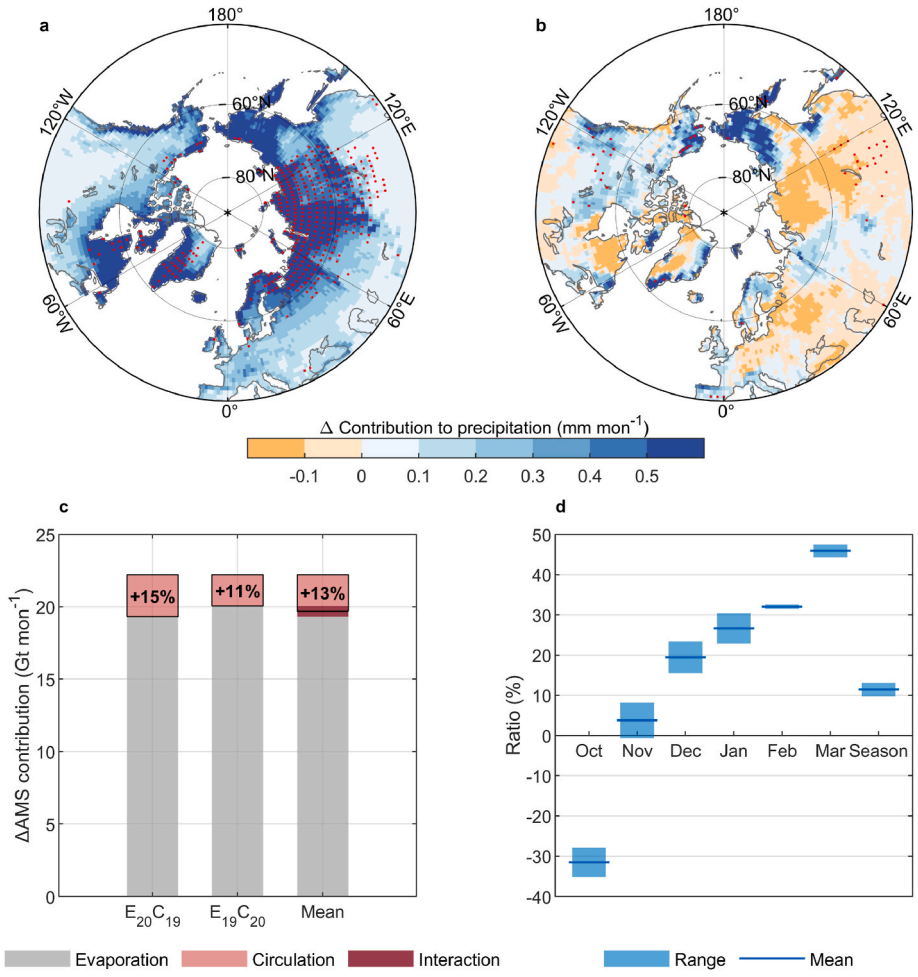


**Fig. 1.** Changes in AMS contribution to precipitation. Differences in AMS moisture contribution to land precipitation driven by changes in (**a**) AMS evaporation and (**b**) atmospheric circulation between the cold seasons of the 1980s and 2010s (2010s minus 1980s). Red stippling denotes areas where the changes attributed to this component are statistically significant ($p < 0.05$) in both sets of comparisons. (**c**) Total change and attribution of AMS moisture contribution to Northern Hemisphere land precipitation. The gap between experiment groups represents evaporation-circulation interaction, while individual contributions are derived from their means (see Methods). Numbers indicate the additional contribution from circulation relative to evaporation. (**d**) Monthly ratios of circulation-induced AMS contribution changes relative to the total changes of AMS-sourced precipitation over Northern Hemisphere land. Boxes show the range between experimental results, with lines indicating their mean values.

prevailing cause of the overall decrease in AMS-sourced precipitation, consistent with the marked decline in local precipitation in Fig. S1a.

Fig. 1d presents the ratio of changes in AMS moisture contribution attributable to atmospheric circulation relative to the total AMS-sourced land precipitation changes in each cold month, highlighting the influence extent of added moisture of atmospheric circulation. The regulatory role of circulation shows obvious monthly variation. The negative value in October indicates that circulation changes suppressed the contribution of Arctic moisture to land precipitation. Such negative contributions occurred across multiple regions within 50–80°N, including the Western and Central Eurasia, Alaksa and Western Canada, and Greenland, weakening the increased contribution driven solely by enhanced AMS evaporation (Fig. S3c). In November, both positive and negative ratios indicate a mixed effect. The consistently positive and rising ratios pointed to an increasingly strong circulation-driven enhancement from December to March. The amplification effect of circulation peaked in March, with a ratio exceeding 45 %. Monthly variations in AMS-sourced precipitation attributable to changes in evaporation and atmospheric circulation are illustrated in Fig. S4 and Fig. S5.

### 3.2. *Atmospheric circulation-driven amplification of AMS contributions to extreme snowfall*

Strongly influenced by the prevalence of sub-freezing temperatures, extreme precipitation events over the circum-Arctic land during the cold season predominantly occur in solid form. Extreme snowfall events were identified as daily snowfall exceeding 10 mm of water equivalent (Lin and Chen, 2022). During such events, snowfall constitutes more than 85 % of total precipitation on average, and exceeds 95 % in high-latitude regions (Fig. S6). Given that extreme winter weather events are primarily associated with snowfall rather than rainfall, the following analysis, focusing specifically on extreme snowfall, allows for a more direct assessment of the increasing risk of disruptive winter weather in response to Arctic changes.

During the 1980s, the average total extreme snowfall across Northern Hemisphere landmasses was 339.9 Gt mon$^{-1}$, which increased by approximately 1 % to 343.1 Gt mon$^{-1}$ in the 2010s. Although the AMS moisture contribution accounts for only 3 % of the total cold-season extreme snowfall, its contribution exhibited a significant increase from 8.6 Gt mon$^{-1}$ ($E_{19}C_{19}$) in the 1980s to 11.6 Gt mon$^{-1}$ ($E_{20}C_{20}$) in the 2010s (Fig. S7). Of this total increase, 1.7 Gt mon$^{-1}$ came from the enhanced evaporation and 1.4 Gt mon$^{-1}$ from circulation changes, with

an estimated interaction effect of ±0.16 Gt mon$^{-1}$ (Fig. 2c). The intensified evaporation enhanced the AMS contribution to extreme snowfall in all affected regions, with particularly pronounced influence along the mid-to-high latitude coasts of the North Pacific and North Atlantic (Fig. 2a).

The effects of circulation changes (Fig. 2b) indicate that extreme snowfall over Greenland, northern Europe, eastern Russia, and the western regions of Canada underwent further enhancements in extra AMS contributions, in addition to the increases driven by enhanced evaporation from areas of sea-ice loss. Notably, in over 78 % of Northern Hemisphere land areas experiencing extreme snowfall, changes in the AMS contribution were more likely to be governed by atmospheric circulation dynamics rather than enhanced moisture availability from source-region evaporation. This is evidenced by the close spatial correspondence between circulation-induced changes (Fig. 2b) and total AMS contribution changes (Fig. S7c). Conversely, circulation changes reduced AMS moisture transport to regions such as western Europe and northeastern Canada, leading to diminished contributions to extreme snowfall in these areas.

The quantitative comparison of the experiments reveals that, while enhanced evaporation intensified the moisture supply, changes in atmospheric circulation further amplified the AMS moisture contribution to extreme snowfall—resulting in an additional 84 % increase relative to the effect of evaporation alone. Consequently, the total increase in AMS moisture in extreme snowfall from the 1980s to the 2010s is attributed to 54 % from enhanced evaporation and 46 % from favorable moisture transport driven by atmospheric circulation changes. The positive effects of circulation are evident throughout all cold months, with its amplifying influence becoming substantially stronger from December to March. During this period, the circulation-induced enhancement accounts for nearly or more than half of the total increase in AMS contribution to extreme snowfall over land, peaking in March with maximum intensification reaching up to 70 % (Fig. 2d). This pronounced role indicates that atmospheric circulation changes can independently enhance AMS moisture transport efficiency to high-latitude land and promote extreme snowfall formation, regardless of evaporation changes.

### 3.3. *The mechanisms of atmospheric circulation changes in altering moisture redistribution and anthropogenic intensification*

The above results show that from December to March, the change in Arctic moisture contribution to land precipitation or extreme snowfall driven by atmospheric circulation remains consistently positive across different experimental results, with its impact notably higher than that observed from October to November. To further elucidate the role of

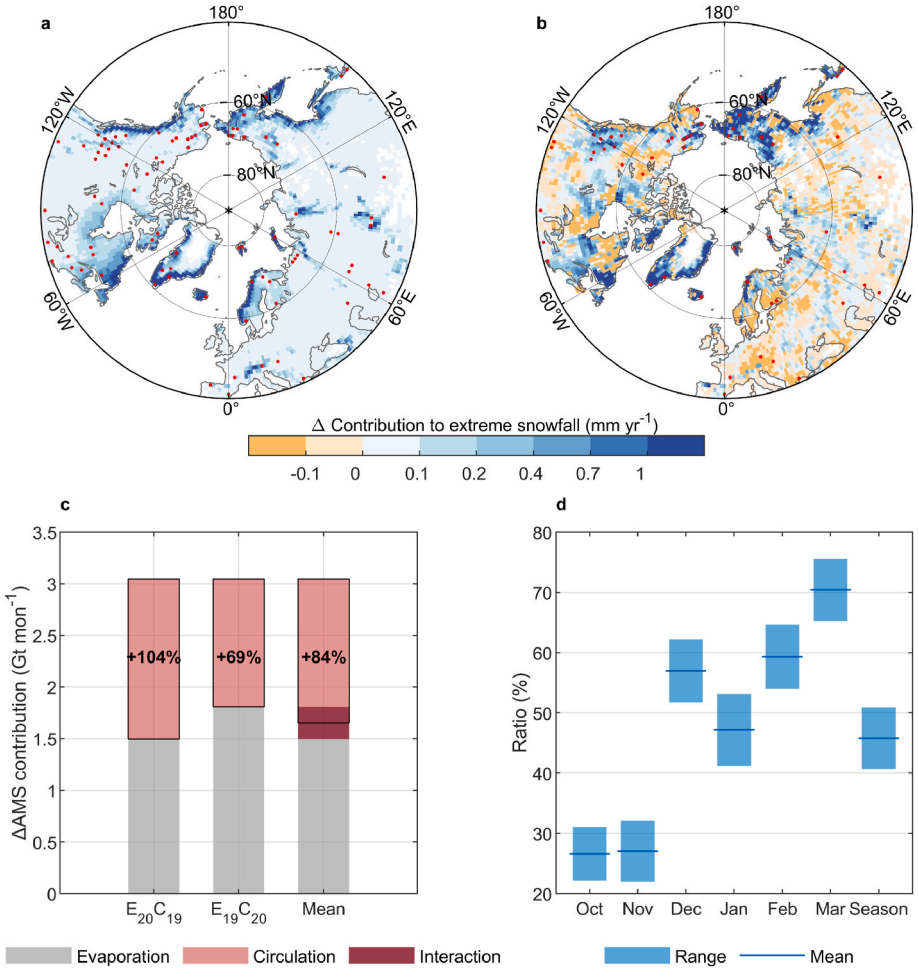


**Fig. 2.** Changes in AMS contribution to extreme snowfall. Differences in AMS moisture contribution to extreme snowfall over land driven by changes in (**a**) AMS evaporation and (**b**) atmospheric circulation between the cold seasons of the 1980s and 2010s (2010s minus 1980s). Red stippling denotes areas where the changes attributed to this component are statistically significant ($p < 0.05$) in both sets of comparisons. (**c**) Total change and attribution of the AMS moisture contribution to extreme snowfall over Northern Hemisphere land. The gap between experiment groups represents evaporation-circulation interaction, while individual contributions are derived from their means. Numbers indicate the additional contribution from circulation relative to evaporation. (**d**) Monthly ratios of circulation-induced AMS contribution changes relative to the total changes in AMS contribution to extreme snowfall over Northern Hemisphere land. Boxes show the range between experimental results, with lines indicating their mean values.

atmospheric circulation changes in regulating the redistribution of AMS moisture, the following sections focus on the atmospheric circulation changes during the period from December to March.

The polar atmospheric column during winter has undergone thermal expansion due to amplified lower-tropospheric warming, accompanied by an increase in 500 hPa geopotential height (Fig. 3a). This rise extends southward from the central Arctic, covering the Scandinavian Peninsula as well as East Siberia. Slight decreases in geopotential height are observed over central Canada and western Siberia compared to the 1980s. A west-to-east gradient in geopotential height changes spanning west Canada and northern Europe facilitated intensified northerly winds, enabling localized southward intrusions of Arctic moisture (Fig. S8b). The weakened geopotential height gradient between the Arctic Ocean and surrounding land areas altered atmospheric flow and led to more meridional meandering across most of the circum-Arctic (Fig. S8), as evidenced by changes in the meridional circulation index (Francis and Vavrus, 2015). On average, strengthened low-level northerly winds north of 70°N (Fig. 3b), along with the precipitable water increased over the Arctic (Fig. 3c), facilitated the southward advection of moist Arctic air onto land. Zonally averaged changes in moisture flux during land extreme snowfall events also reveal more southward transport that enhanced Arctic moisture contributions (Fig. 3d).

Our results suggest that changes in pressure structures and moisture distribution of the extratropical atmospheric patterns constituted a key driver of the enhanced land moistening associated with sea-ice retreat. However, given the notable circulation anomalies contributed by natural variability (Ma et al., 2024; Zhou et al., 2024), further testing is required to determine whether changes in Arctic atmospheric circulation represent a significant response to climate change driven by anthropogenic forcing. To that end, we analyzed outputs from 32 simulations of the historical and SSP2-4.5 scenarios from the CMIP6. The potential climate change signals in the Arctic atmospheric circulation were highlighted by averaging out the noise generated by internal climate variability and intermodel uncertainty. For integrated water vapor averaged over the high-latitude region (60–80°N), the CMIP6 multi-model mean and ERA5 exhibit close and significant increases (Fig. 4a), with 0.12 mm dec$^{-1}$ anthropogenic forcing influence and 0.09 mm dec$^{-1}$ observed increasing slope. Regions with maximum increases show strong spatial coherence, such as the rise over the Barents and Norwegian Seas (Fig. S9a and b). The geopotential height increase was evident in both the ERA5 and CMIP6 results, with enhanced geopotential height extending from the central Arctic toward Greenland (Fig. S9c and d). While a discrepancy emerged over mid-latitude land, with ERA5 indicating a slight decrease, whereas the CMIP6 ensemble mean suggests an increase. On the whole, the expansion over the Arctic Ocean was more dramatic than over the land regions, leading to the weakened pressure gradient between the polar region and surrounding land areas (Fig. 4b). CMIP6 detected an anthropogenic forcing signal in

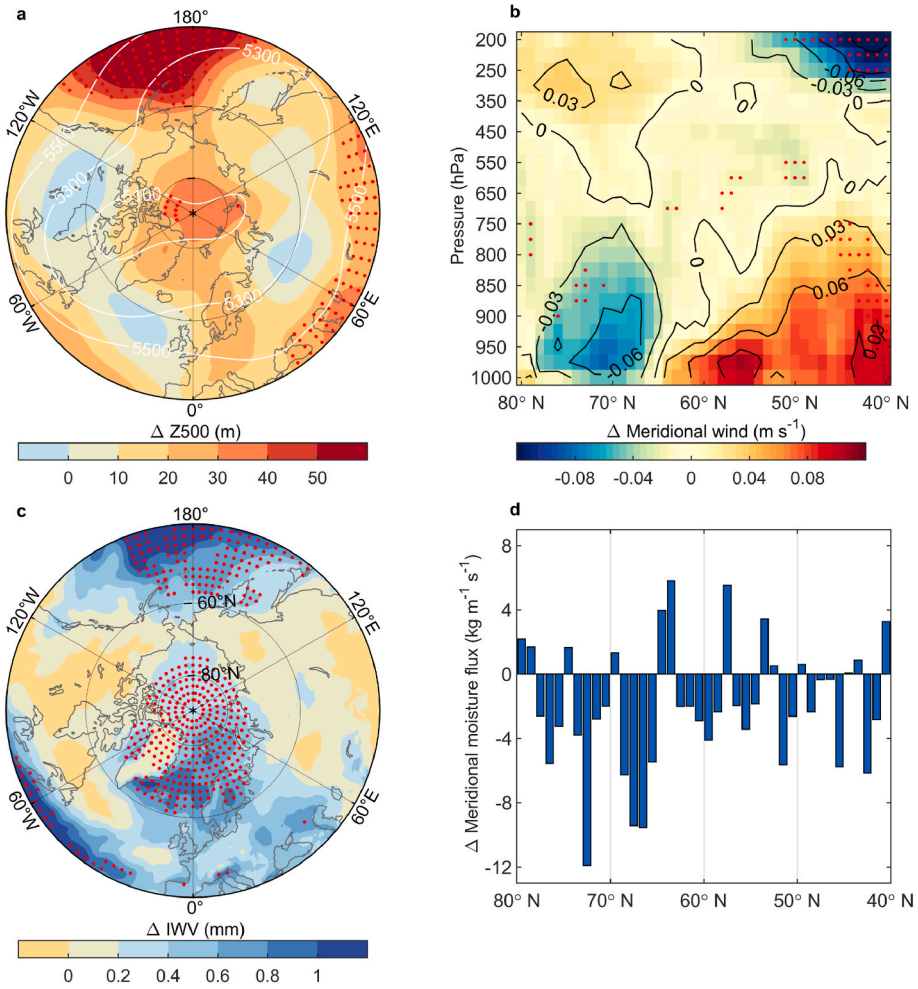


**Fig. 3.** Changes in atmospheric conditions during December211; March. Changes in (**a**) 500-hPa geopotential height, (**b**) meridional wind across pressure levels and latitudes, and (**c**) integrated water vapor (IWV) between the 2010s and the 1980s (2010s minus 1980s). Red stippling denotes areas where the changes attributed to this component are statistically significant ($p < 0.05$). (**d**) Changes in zonally averaged total column vertically-integrated meridional water vapor flux over land during the extreme snowfall events between the 2010s and the 1980s. In panels (**b**) and (**d**), negative meridional values denote intensified southward transport, whereas positive values denote intensified northward transport.

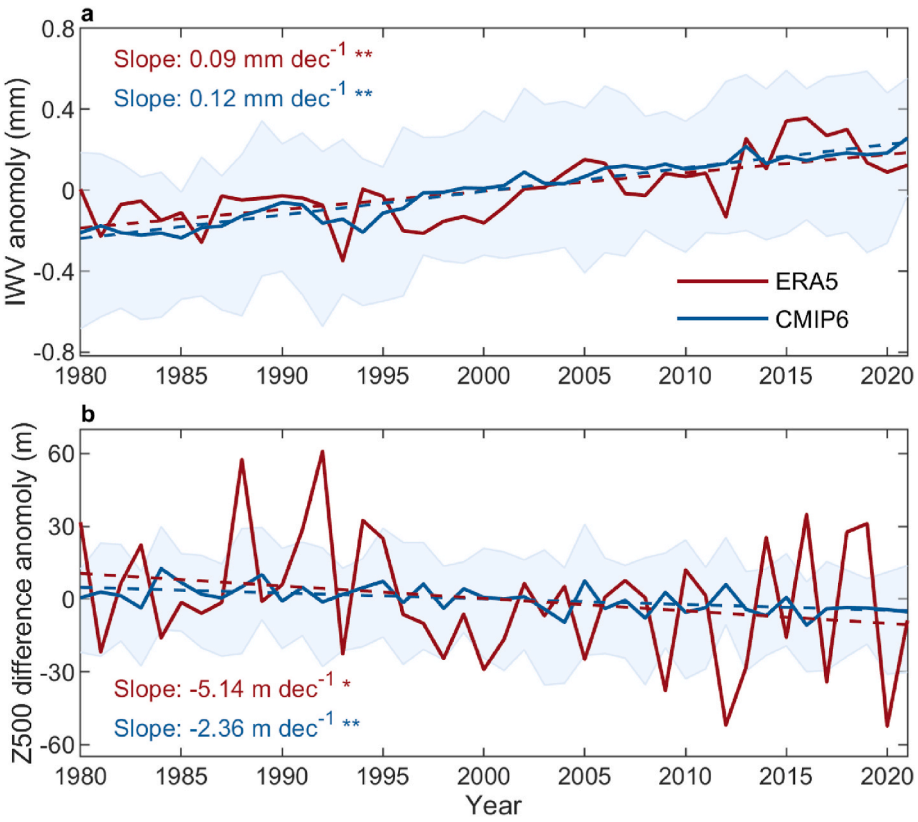


**Fig. 4.** Changes in atmospheric circulation driven by anthropogenic forcing. (**a**) Anomalies of the 60–80°N average integrated water vapor (IWV), and (**b**) anomalies in the 500-hPa geopotential height difference between 60 and 70°N land and 70–90°N. during the 1980–2021 cold seasons based on ERA5 (red lines) and CMIP6 multi-model ensemble mean (blue lines). The solid lines represent the time series, the dashed lines show the fitted trends, and the blue shading indicates the interquartile range (25th to 75th percentile) across all CMIP6 models. ** and * indicate slopes significant at the $p < 0.05$ and $p < 0.1$ levels.

this change, with the geopotential height difference significantly decreasing at a rate of 2.4 m dec$^{-1}$. Consistent trends across the CMIP6 multi-model ensemble confirm that changes in Arctic atmospheric circulation are strongly associated with responses to anthropogenic forcing.

## 4. Discussion and conclusions

The response of the Arctic water cycle to climate change is often attributed to thermodynamics processes, particularly enhanced evaporation from ice-free seas and increased atmospheric water vapor capacity as described by the Clausius–Clapeyron relationship. However, dynamic processes, such as changes in atmospheric circulation, also play a critical role in shaping regional climate patterns (Hori et al., 2024). Despite their importance, our understanding of these dynamic influences remains limited due to the complexity of the climate system (Shepherd, 2014). To disentangle these effects, we used an offline moisture-tracing model forced with separate evaporation and circulation inputs to isolate and quantify their relative contributions to changes in AMS-sourced precipitation. Our results show that the increase in AMS-sourced precipitation scales approximately with the enhancement of AMS evaporation. However, for extreme snowfall, shifts in AMS moisture contribution more closely follow the pattern induced by atmospheric circulation changes. In such events, the landward AMS moisture accumulation driven by circulation changes can even exceed the contribution from increased evaporation alone.

While our approach allows for a controlled assessment of the individual contributions, the offline model framework inherently prevents dynamic feedback between evaporation and circulation within individual simulations. In reality, these processes are tightly coupled: changes in evaporation can alter atmospheric heat and moisture transport (Fajber et al., 2023), while circulation patterns influence Arctic evaporation through wind speed, temperature gradients, and sea-ice movement (McVicar et al., 2012; Nygård et al., 2019; Pavlova et al., 2014). To address this, our experimental design includes complementary comparisons that interpret differences across simulations as varying degrees of coupled response. However, more advanced coupled modelling frameworks are needed to quantify the full extent of these evaporation–circulation interactions.

Despite the typical expectation of smaller precipitation increases over land than over oceans under warming (Allan et al., 2020), changes in Arctic atmospheric circulation have promoted AMS moisture transport to land, which could contribute to the comparable high-latitude net precipitation over both land and ocean. This has led to a higher proportion of AMS-sourced precipitation falling over land and a corresponding decrease over oceans. Circulation-driven changes in moisture transport contributed 11 % of the total increase in AMS-sourced land precipitation. Notably, during extreme snowfall events, enhanced landward moisture transport driven by atmospheric circulation added 84 % more AMS-sourced snowfall beyond the contribution from increased evaporation alone. This highlights the key role of circulation in amplifying Arctic moisture contributions to extreme weather.

Cyclonic circulation—identified by the 985 hPa threshold in instantaneous sea-level pressure over pan-Arctic (Rinke et al., 2017)—is responsible for over half of extreme snowfall events in coastal regions (Fig. S10a). This finding is consistent with recent studies linking extreme precipitation to cyclonic activity (Bailey and Hubbard, 2025; Müller et al., 2022; Sato et al., 2022; Serreze et al., 2022). The rising frequency of such low-pressure-induced snowfall in regions such as Norway, western and eastern Russia, eastern Canada, and the eastern coast of Greenland reflects an intensified ocean-to-land moisture influx that fuels localized snowfall upon landfall (Fig. S10b and c). Meanwhile, a

strengthening of anticyclonic circulation over the Barents–Kara Seas has reduced low-pressure systems over Eastern Europe, while enhancing moisture convergence to the west (Liu et al., 2025). Furthermore, changes in the proportion of AMS-sourced moisture in regional snowfall also indicates more efficient conversion to coastal extreme snowfall than before (Fig. S10d), supporting previous findings that transient eddies are the main carriers of moisture away from marginal ice zones near the North Atlantic (Hori et al., 2024).

In response to sea-ice loss and Arctic warming, coupled model experiments consistently show a winter atmospheric circulation trend marked by weakened westerlies on the polar side (Screen et al., 2018). This weakening slows the eastward propagation of large-scale Rossby waves and increases their amplitude (Francis and Vavrus, 2012; Martin, 2021). As a result, cyclonic Rossby wave-breaking events drive southward advection of AMS moisture via transient eddies, reshaping regional moisture transport (Hori et al., 2024; McGraw et al., 2020). These circulation adjustments, driven by anthropogenic forcing, enhance local moisture contributions and build upon large-scale moistening from increased evaporation.

As Arctic sea ice continues to retreat and atmospheric circulation patterns evolve under climate change, anthropogenic forcing is increasingly recognized as a key driver of high-latitude hydrological changes. Our findings deepen the understanding of the Arctic water cycle's response to ongoing warming and provide insights that may improve projections of high-latitude precipitation and extreme events.

## CRediT authorship contribution statement

**Yubo Liu:** Writing – original draft, Methodology, Conceptualization. **Qiuhong Tang:** Writing – review & editing, Conceptualization. **L. Ruby Leung:** Conceptualization. **Deliang Chen:** Writing – review & editing. **Jennifer A. Francis:** Writing – review & editing. **Chi Zhang:** Writing – review & editing, Methodology. **Hans W. Chen:** Writing – review & editing. **Steven C. Sherwood:** Writing – review & editing, Methodology.

## Code availability

The Water Accounting Model-2 layers (WAM-2layers) moisture tracking scheme in Python code is available from https://github.com/ruudvdent/WAM2layersPython. All code necessary for performing the analyses is available upon request from the corresponding authors.

## Declaration of competing interest

The authors declare that they have no known competing financial interests or personal relationships that could have appeared to influence the work reported in this paper.

## Acknowledgements

This study was supported by the National Natural Science Foundation of China (U2243226), Third Xinjiang Scientific Expedition Program (2021xjkk0800) and NSFC-DFG mobility (M-0468). Y.L. was supported by the China Scholarship Council. D.C. was supported by Tsinghua University (100008001). L.R.L. was supported by the Office of Science, U.S. Department of Energy, Biological and Environmental Research as part of the Regional and Global Model Analysis program area. PNNL is operated for the Department of Energy by Battelle Memorial Institute under contract DE-AC05-76RL01830.

## Appendix A. Supplementary data

Supplementary data to this article can be found online at https://doi.org/10.1016/j.wace.2025.100802.

## Data availability

ERA5 reanalysis data are available from https://doi.org/10.24381/cds.bd0915c6 and https://doi.org/10.24381/cds.adbb2d47. CMIP6 data are available from https://esgf-node.llnl.gov/search/cmip6/.

## References

Allan, R.P., Barlow, M., Byrne, M.P., Cherchi, A., Douville, H., Fowler, H.J., Gan, T.Y., Pendergrass, A.G., Rosenfeld, D., Swann, A.L.S., Wilcox, L.J., Zolina, O., 2020. Advances in understanding large-scale responses of the water cycle to climate change. Ann. N. Y. Acad. Sci. 1472, 49–75. https://doi.org/10.1111/nyas.14337.

Avila-Diaz, A., Bromwich, D.H., Wilson, A.B., Justino, F., Wang, S.-H., 2021. Climate extremes across the north American Arctic in modern reanalyses. J. Clim. 34, 2385–2410. https://doi.org/10.1175/JCLI-D-20-0093.1.

Bailey, H., Hubbard, A., 2025. Snow mass recharge of the Greenland ice sheet fueled by intense atmospheric river. Geophys. Res. Lett. 52, e2024GL110121. https://doi.org/10.1029/2024GL110121.

Bailey, H., Hubbard, A., Klein, E.S., Mustonen, K.-R., Akers, P.D., Marttila, H., Welker, J. M., 2021. Arctic sea-ice loss fuels extreme European snowfall. Nat. Geosci. 14, 283–288. https://doi.org/10.1038/s41561-021-00719-y.

Barrett, A.P., Stroeve, J.C., Serreze, M.C., 2020. Arctic Ocean precipitation from atmospheric reanalyses and comparisons with north pole drifting station records. J. Geophys. Res.: Oceans 125, e2019JC015415. https://doi.org/10.1029/2019JC015415.

Bintanja, R., Selten, F.M., 2014. Future increases in Arctic precipitation linked to local evaporation and sea-ice retreat. Nature 509, 479–482. https://doi.org/10.1038/nature13259.

Boisvert, L.N., Stroeve, J.C., 2015. The Arctic is becoming warmer and wetter as revealed by the Atmospheric Infrared Sounder. Geophys. Res. Lett. 42, 4439–4446. https://doi.org/10.1002/2015GL063775.

Cai, Z., You, Q., Chen, H.W., Zhang, R., Zuo, Z., Chen, D., Cohen, J., Screen, J.A., 2024. Assessing Arctic wetting: performances of CMIP6 models and projections of precipitation changes. Atmos. Res. 297, 107124. https://doi.org/10.1016/j.atmosres.2023.107124.

Choi, H.-J., Min, S.-K., Yeh, S.-W., An, S.-I., Kim, B.-M., 2023. Seasonally distinct contributions of greenhouse gases and anthropogenic aerosols to historical changes in Arctic moisture budget. npj Clim. Atmos. Sci. 6, 1–14. https://doi.org/10.1038/s41612-023-00518-9.

Chripko, S., Msadek, R., Sanchez-Gomez, E., Terray, L., Bessières, L., Moine, M.-P., 2021. Impact of reduced Arctic Sea ice on Northern hemisphere climate and weather in autumn and Winter. J. Clim. 34, 5847–5867. https://doi.org/10.1175/JCLI-D-20-0515.1.

Crawford, A.D., Lukovich, J.V., McCrystall, M.R., Stroeve, J.C., Barber, D.G., 2022. Reduced sea ice enhances intensification of winter storms over the Arctic Ocean. J. Clim. 35, 3353–3370. https://doi.org/10.1175/JCLI-D-21-0747.1.

Dial, R.J., Maher, C.T., Hewitt, R.E., Wockenfuss, A.M., Wong, R.E., Crawford, D.J., Zietlow, M.G., Sullivan, P.F., 2024. Arctic sea ice retreat fuels boreal forest advance. Science 383, 877–884. https://doi.org/10.1126/science.adh2339.

Ding, Q., Schweiger, A., L'Heureux, M., Steig, E.J., Battisti, D.S., Johnson, N.C., Blanchard-Wrigglesworth, E., Po-Chedley, S., Zhang, Q., Harnos, K., Bushuk, M., Markle, B., Baxter, I., 2019. Fingerprints of internal drivers of Arctic sea ice loss in observations and model simulations. Nat. Geosci. 12, 28–33. https://doi.org/10.1038/s41561-018-0256-8.

Dufour, A., Zolina, O., Gulev, S.K., 2016. Atmospheric moisture transport to the arctic: assessment of reanalyses and analysis of transport components. J. Clim. 29, 5061–5081. https://doi.org/10.1175/JCLI-D-15-0559.1.

Fajber, R., Donohoe, A., Ragen, S., Armour, K.C., Kushner, P.J., 2023. Atmospheric heat transport is governed by meridional gradients in surface evaporation in modern-day earth-like climates. Proc. Natl. Acad. Sci. 120, e2217202120. https://doi.org/10.1073/pnas.2217202120.

Ford, V.L., Frauenfeld, O.W., 2022. Arctic precipitation recycling and hydrologic budget changes in response to sea ice loss. Global Planet. Change 209, 103752. https://doi.org/10.1016/j.gloplacha.2022.103752.

Francis, J.A., Vavrus, S.J., 2015. Evidence for a wavier jet stream in response to rapid Arctic warming. Environ. Res. Lett. 10, 014005. https://doi.org/10.1088/1748-9326/10/1/014005.

Francis, J.A., Vavrus, S.J., 2012. Evidence linking Arctic amplification to extreme weather in mid-latitudes. Geophys. Res. Lett. 39. https://doi.org/10.1029/2012GL051000.

Ghatak, D., Miller, J., 2013. Implications for Arctic amplification of changes in the strength of the water vapor feedback. J. Geophys. Res. Atmos. 118, 7569–7578. https://doi.org/10.1002/jgrd.50578.

Gimeno, L., Eiras-Barca, J., Durán-Quesada, A.M., Dominguez, F., van der Ent, R., Sodemann, H., Sánchez-Murillo, R., Nieto, R., Kirchner, J.W., 2021. The residence time of water vapour in the atmosphere. Nat. Rev. Earth Environ. 2, 558–569. https://doi.org/10.1038/s43017-021-00181-9.

Graham, R.M., Hudson, S.R., Maturilli, M., 2019. Improved performance of ERA5 in Arctic gateway relative to four global atmospheric reanalyses. Geophys. Res. Lett. 46, 6138–6147. https://doi.org/10.1029/2019GL082781.

Hersbach, H., Bell, B., Berrisford, P., Hirahara, S., Horányi, A., Muñoz-Sabater, J., Nicolas, J., Peubey, C., Radu, R., Schepers, D., Simmons, A., Soci, C., Abdalla, S.,

Abellan, X., Balsamo, G., Bechtold, P., Biavati, G., Bidlot, J., Bonavita, M., Chiara, G., Dahlgren, P., Dee, D., Diamantakis, M., Dragani, R., Flemming, J., Forbes, R., Fuentes, M., Geer, A., Haimberger, L., Healy, S., Hogan, R.J., Hólm, E., Janisková, M., Keeley, S., Laloyaux, P., Lopez, P., Lupu, C., Radnoti, G., Rosnay, P., Rozum, I., Vamborg, F., Villaume, S., Thépaut, J., 2020. The ERA5 global reanalysis. Q. J. R. Meteorol. Soc. 146, 1999–2049. https://doi.org/10.1002/qj.3803.

Hori, M.E., Yoshimori, M., Ukita, J., 2024. Changing role of horizontal moisture advection in the lower troposphere under extreme Arctic amplification. Geophys. Res. Lett. 51, e2024GL109299. https://doi.org/10.1029/2024GL109299.

Kretschmer, M., Zappa, G., Shepherd, T.G., 2020. The role of Barents–Kara sea ice loss in projected polar vortex changes. Weather Clim. Dynam. 1, 715–730. https://doi.org/10.5194/wcd-1-715-2020.

Levine, X.J., Cvijanovic, I., Ortega, P., Donat, M.G., Tourigny, E., 2021. Atmospheric feedback explains disparate climate response to regional Arctic sea-ice loss. npj Clim. Atmos. Sci. 4, 1–8. https://doi.org/10.1038/s41612-021-00183-w.

Lin, W., Chen, H., 2022. Changes in the spatial–temporal characteristics of daily snowfall events over the Eurasian continent from 1980 to 2019. Int. J. Climatol. 42, 1841–1853. https://doi.org/10.1002/joc.7339.

Liu, J., Curry, J.A., Wang, H., Song, M., Horton, R.M., 2012. Impact of declining Arctic sea ice on winter snowfall. Proc. Natl. Acad. Sci. USA 109, 4074–4079. https://doi.org/10.1073/pnas.1114910109.

Liu, Y., Tang, Q., Zhang, C., Chen, D., Francis, J.A., Leung, L.R., Chen, H.W., 2024. The disproportionate impact of enhanced evaporation from melting arctic sea ice on cold-season land precipitation trends. npj Clim. Atmos. Sci. 7, 1–9. https://doi.org/10.1038/s41612-024-00680-8.

Liu, Z., Risi, C., Codron, F., Gastineau, G., Huan, X., Lan, H., Xu, W., Bowen, G.J., 2025. Anthropogenic intensification of Arctic anticyclonic circulation. Sci. Adv. 11, eads4508. https://doi.org/10.1126/sciadv.ads4508.

Liu, Z., Risi, C., Codron, F., Jian, Z., Wei, Z., He, X., Poulsen, C.J., Wang, Y., Chen, D., Ma, W., Cheng, Y., Bowen, G.J., 2022. Atmospheric forcing dominates winter Barents-Kara sea ice variability on interannual to decadal time scales. Proc. Natl. Acad. Sci. USA 119, e2120770119. https://doi.org/10.1073/pnas.2120770119.

Luo, B., Luo, D., Dai, A., Xiao, C., Simmonds, I., Hanna, E., Overland, J., Shi, J., Chen, X., Yao, Y., Duan, W., Liu, Y., Zhang, Q., Xu, X., Diao, Y., Jiang, Z., Gong, T., 2024. Rapid summer Russian Arctic sea-ice loss enhances the risk of recent Eastern Siberian wildfires. Nat. Commun. 15, 5399. https://doi.org/10.1038/s41467-024-49677-0.

Ma, W., Wang, H., Chen, G., Leung, L.R., Lu, J., Rasch, P.J., Fu, Q., Kravitz, B., Zou, Y., Cassano, J.J., Maslowski, W., 2024. The role of interdecadal climate oscillations in driving Arctic atmospheric river trends. Nat. Commun. 15, 2135. https://doi.org/10.1038/s41467-024-45159-5.

Martin, J.E., 2021. Recent trends in the waviness of the Northern hemisphere wintertime polar and subtropical jets. J. Geophys. Res. Atmos. 126, e2020JD033668. https://doi.org/10.1029/2020JD033668.

McCrystall, M.R., Stroeve, J., Serreze, M., Forbes, B.C., Screen, J.A., 2021. New climate models reveal faster and larger increases in Arctic precipitation than previously projected. Nat. Commun. 12, 6765. https://doi.org/10.1038/s41467-021-27031-y.

McGraw, M.C., Baggett, C.F., Liu, C., Mundhenk, B.D., 2020. Changes in Arctic moisture transport over the North Pacific associated with sea ice loss. Clim. Dyn. 54, 491–506. https://doi.org/10.1007/s00382-019-05011-9.

McVicar, T.R., Roderick, M.L., Donohue, R.J., Li, L.T., Van Niel, T.G., Thomas, A., Grieser, J., Jhajharia, D., Himri, Y., Mahowald, N.M., Mescherskaya, A.V., Kruger, A. C., Rehman, S., Dinpashoh, Y., 2012. Global review and synthesis of trends in observed terrestrial near-surface wind speeds: implications for evaporation. J. Hydrol. 416–417, 182–205. https://doi.org/10.1016/j.jhydrol.2011.10.024.

Müller, M., Kelder, T., Palerme, C., 2022. Decline of sea-ice in the Greenland Sea intensifies extreme precipitation over Svalbard. Weather Clim. Extrem. 36, 100437. https://doi.org/10.1016/j.wace.2022.100437.

Nygård, T., Graversen, R.G., Uotila, P., Naakka, T., Vihma, T., 2019. Strong dependence of wintertime Arctic moisture and cloud distributions on atmospheric large-scale circulation. J. Clim. 32, 8771–8790. https://doi.org/10.1175/JCLI-D-19-0242.1.

Papritz, L., Hauswirth, D., Hartmuth, K., 2022. Moisture origin, transport pathways, and driving processes of intense wintertime moisture transport into the Arctic. Weather Clim. Dynam. 3, 1–20. https://doi.org/10.5194/wcd-3-1-2022.

Pavlova, O., Pavlov, V., Gerland, S., 2014. The impact of winds and sea surface temperatures on the Barents Sea ice extent, a statistical approach. J. Mar. Syst. 130, 248–255. https://doi.org/10.1016/j.jmarsys.2013.02.011.

Pithan, F., Jung, T., 2021. Arctic amplification of precipitation changes—The energy Hypothesis. Geophys. Res. Lett. 48, e2021GL094977. https://doi.org/10.1029/2021GL094977.

Ridley, J.K., Blockley, E.W., Ringer, M.A., 2023. Arctic Sea ice causes seasonal differences in the response of Arctic water vapor to climate warming in the CMIP6 model, HadGEM3-GC3.1. Geophys. Res. Lett. 50, e2022GL102541. https://doi.org/10.1029/2022GL102541.

Rinke, A., Maturilli, M., Graham, R.M., Matthes, H., Handorf, D., Cohen, L., Hudson, S.R., Moore, J.C., 2017. Extreme cyclone events in the Arctic: Wintertime variability and trends. Environ. Res. Lett. 12, 094006. https://doi.org/10.1088/1748-9326/aa7def.

Sato, T., Nakamura, T., Iijima, Y., Hiyama, T., 2022. Enhanced Arctic moisture transport toward Siberia in autumn revealed by tagged moisture transport model experiment. npj Clim. Atmos. Sci. 5, 1–7. https://doi.org/10.1038/s41612-022-00310-1.

Screen, J.A., Deser, C., Smith, D.M., Zhang, X., Blackport, R., Kushner, P.J., Oudar, T., McCusker, K.E., Sun, L., 2018. Consistency and discrepancy in the atmospheric response to Arctic sea-ice loss across climate models. Nat. Geosci. 11, 155–163. https://doi.org/10.1038/s41561-018-0059-y.

Sellevold, R., Lenaerts, J.T.M., Vizcaino, M., 2022. Influence of Arctic sea-ice loss on the Greenland ice sheet climate. Clim. Dyn. 58, 179–193. https://doi.org/10.1007/s00382-021-05897-4.

Serreze, M.C., Voveris, J., Barrett, A.P., Fox, S., Blanken, P.D., Crawford, A., 2022. Characteristics of extreme daily precipitation events over the Canadian Arctic. Int. J. Climatol. 42, 10353–10372. https://doi.org/10.1002/joc.7907.

Shepherd, T.G., 2014. Atmospheric circulation as a source of uncertainty in climate change projections. Nat. Geosci. 7, 703–708. https://doi.org/10.1038/ngeo2253.

Smith, D.M., Eade, R., Andrews, M.B., Ayres, H., Clark, A., Chripko, S., Deser, C., Dunstone, N.J., García-Serrano, J., Gastineau, G., Graff, L.S., Hardiman, S.C., He, B., Hermanson, L., Jung, T., Knight, J., Levine, X., Magnusdottir, G., Manzini, E., Matei, D., Mori, M., Msadek, R., Ortega, P., Peings, Y., Scaife, A.A., Screen, J.A., Seabrook, M., Semmler, T., Sigmond, M., Streffing, J., Sun, L., Walsh, A., 2022. Robust but weak winter atmospheric circulation response to future Arctic sea ice loss. Nat. Commun. 13, 727. https://doi.org/10.1038/s41467-022-28283-y.

Stroeve, J., Notz, D., 2018. Changing state of Arctic sea ice across all seasons. Environ. Res. Lett. 13, 103001. https://doi.org/10.1088/1748-9326/aade56.

Stroeve, J.C., Serreze, M.C., Holland, M.M., Kay, J.E., Malanik, J., Barrett, A.P., 2012. The Arctic's rapidly shrinking sea ice cover: a research synthesis. Clim. Change 110, 1005–1027. https://doi.org/10.1007/s10584-011-0101-1.

Topál, D., Ding, Q., 2023. Atmospheric circulation-constrained model sensitivity recalibrates Arctic climate projections. Nat. Clim. Chang. 13, 710–718. https://doi.org/10.1038/s41558-023-01698-1.

van der Ent, R.J., Tuinenburg, O.A., Knoche, H.-R., Kunstmann, H., Savenije, H.H.G., 2013. Should we use a simple or complex model for moisture recycling and atmospheric moisture tracking? Hydrol. Earth Syst. Sci. 17, 4869–4884. https://doi.org/10.5194/hess-17-4869-2013.

van der Ent, R.J., Wang-Erlandsson, L., Keys, P.W., Savenije, H.H.G., 2014. Contrasting roles of interception and transpiration in the hydrological cycle – part 2: moisture recycling. Earth Syst. Dynam. 5, 471–489. https://doi.org/10.5194/esd-5-471-2014.

Vázquez, M., Nieto, R., Drumond, A., Gimeno, L., 2016. Moisture transport into the Arctic: source-receptor relationships and the roles of atmospheric circulation and evaporation. J. Geophys. Res. Atmos. 121, 13493–13509. https://doi.org/10.1002/2016JD025400.

Wegmann, M., Orsolini, Y., Vázquez, M., Gimeno, L., Nieto, R., Bulygina, O., Jaiser, R., Handorf, D., Rinke, A., Dethloff, K., Sterin, A., Brönnimann, S., 2015. Arctic moisture source for Eurasian snow cover variations in autumn. Environ. Res. Lett. 10, 054015. https://doi.org/10.1088/1748-9326/10/5/054015.

Yu, Q., Wu, B., Zhang, W., 2024. The atmospheric connection between the Arctic and Eurasia is underestimated in simulations with prescribed sea ice. Commun. Earth Environ. 5, 1–10. https://doi.org/10.1038/s43247-024-01605-2.

Zapponini, M., Goessling, H.F., 2024. Atmospheric destabilization leads to Arctic Ocean winter surface wind intensification. Commun. Earth Environ. 5, 1–9. https://doi.org/10.1038/s43247-024-01428-1.

Zhang, C., Chen, D., Li, L., Liu, X., Cui, H., 2017. Tracing changes in atmospheric moisture supply to the drying Southwest China. Atmos. Chem. Phys. 17, 10383–10393. https://doi.org/10.5194/acp-17-10383-2017.

Zhou, W., Leung, L.R., Lu, J., 2024. Steady threefold Arctic amplification of externally forced warming masked by natural variability. Nat. Geosci. 17, 508–515. https://doi.org/10.1038/s41561-024-01441-1.

Zou, C., Zhang, R., 2024. Arctic Sea ice loss modulates the surface impact of autumn stratospheric polar vortex stretching events. Geophys. Res. Lett. 51, e2023GL107221. https://doi.org/10.1029/2023GL107221.